90º Skew Leading Edge Film Cooling Effectiveness, Heat Transfer, and Discharge Coefficients for Cylindrical Film Holes at High Free Stream Turbulence

Shichuan Ou and Richard Rivir
Air Force Research Laboratory, Propulsion Directorate
1950 Fifth St, WPAFB, Ohio, 45433-7251, USA

ABSTRACT

This paper studies the film effectiveness and heat transfer coefficients on a large scale symmetric circular leading edge with three rows of film holes. The film hole configuration focuses on a smaller injection angle of 20º and a larger hole pitch with respect to the hole diameter (P/d=7.86). The study includes four blowing ratios (M=1.0, 1.5, 2.0 and 2.5), two Reynolds numbers (Re=30,000 and 60,000), and two free stream turbulence levels (approximately Tu=1% and 20% depending on the Reynolds number). The measured discharge coefficients of the film holes were 0.62 - 0.69 and 0.39 - 0.54 at the stagnation row and 0.54 - 0.59 and 0.47 – 0.52 at 21.5º the row, for the range of blowing ratios investigated and Re's of 60,000 and 30,000 respectively. A transient liquid crystal technique was used to obtain the film cooling effectiveness and the heat transfer coefficients. The distributions of film effectiveness and heat transfer coefficient are obtained with spatial resolutions of 0.6 mm or 13% of the film cooling hole diameter. Results are presented for detailed and spanwise averaged values of film effectiveness and Frössling number. Blowing ratios investigated result in up to 2.8 times the lowest blowing ratio's film effectiveness. Increasing the Reynolds number from 30,000 to 60,000 results in increasing the effectiveness by up to 55% at high (20%) turbulence. Turbulence intensity has up to a 60% attenuation on effectiveness between rows at Re = 30,000. The turbulence intensity has the same order of magnitude but opposite effect as Reynolds number, which also has the same order of magnitude effect as blowing ratio on the film effectiveness. A crossover from attenuation to improved film effectiveness after the second row of film holes is found for the high turbulence case as blowing ratio increases. The blowing ratio of two shows a spatial coupling of the stagnation row of film holes with the second row (21.5º) of film holes, which results in the highest film effectiveness and also the highest Frössling numbers.

NOMENCLATURE

A	total area of one row of film holes, cm^2
b	diameter of blown grid tube, 15.88 mm
C_D	Discharge Coefficient = m_a / m_{id}
c_p	specific heat, kJ/kg°C
d	film hole diameter, 4.76 mm
D	leading edge diameter, 8.89 cm
η	film effectiveness
γ	Ratio of specific heats, = 1.4
h	heat transfer coefficient
k	thermal conductivity, w/m°C
$\dot{m}$	mass flow rate of film, kg/sec
M	blowing ratio, $\rho_c U_c/\rho_\infty U_\infty$
N	number of steps
Nu	Nusselt number, hD/k
P	hole pitch, distance between row hole centers
p_e	static pressure at film hole exit, N/.m^2
P_t	total pressure in film cavity, N/ m^2
R	gas constant
Re	Reynolds number based on leading edge diameter, D
Re_d	Reynolds number based on film hole diameter, d
t	time, seconds
T_t	total temperature in film cavity, ºC
Tu	free stream turbulence intensity
U	unit function (in equations 13-16)
U_c	coolant velocity, m/sec
U_∞	free stream velocity, m/sec
x	streamwise distance from blown grid
X	surface distance from the stagnation line
Z	spanwise (lateral) coordinate
α	thermal diffusivity, m^2/sec
Λ	integral scale of turbulence
λ	micro scale of turbulence
δ	boundary layer thickness
ρ_∞	free stream density, kg/m^3
ρ_c	coolant density, kg/m^3

Subscripts

c	coolant
f	film
i	initial
id	Ideal
is	Isentropic
m	mainstream
w	wall

Paper presented at the RTO AVT Symposium on "Advanced Flow Management: Part B – Heat Transfer and Cooling in Propulsion and Power Systems", held in Loen, Norway, 7-11 May 2001, and published in RTO-MP-069(I).

Report Documentation Page

Form Approved
OMB No. 0704-0188

1. REPORT DATE	2. REPORT TYPE	3. DATES COVERED
00 MAR 2003	**N/A**	**-**

4. TITLE AND SUBTITLE	5a. CONTRACT NUMBER
Ninety Degree Skew Leading Edge Film Cooling Effectiveness, Heat Transfer, and Discharge Coefficients for Cylindrical Film Holes at High Free Stream Turbulence	5b. GRANT NUMBER
	5c. PROGRAM ELEMENT NUMBER
6. AUTHOR(S)	5d. PROJECT NUMBER
	5e. TASK NUMBER
	5f. WORK UNIT NUMBER
7. PERFORMING ORGANIZATION NAME(S) AND ADDRESS(ES) **NATO Research and Technology Organisation BP 25, 7 Rue Ancelle, F-92201 Neuilly-Sue-Seine Cedex, France**	8. PERFORMING ORGANIZATION REPORT NUMBER
9. SPONSORING/MONITORING AGENCY NAME(S) AND ADDRESS(ES)	10. SPONSOR/MONITOR'S ACRONYM(S)
	11. SPONSOR/MONITOR'S REPORT NUMBER(S)

12. DISTRIBUTION/AVAILABILITY STATEMENT
Approved for public release, distribution unlimited

13. SUPPLEMENTARY NOTES
Also see ADM001490, presented at RTO Applied Vehicle Technology Panel (AVT) Symposium held in Leon, Norway on 7-11 May 2001, The original document contains color images.

14. ABSTRACT

15. SUBJECT TERMS

16. SECURITY CLASSIFICATION OF:			17. LIMITATION OF ABSTRACT	18. NUMBER OF PAGES	19a. NAME OF RESPONSIBLE PERSON
a. REPORT	b. ABSTRACT	c. THIS PAGE			
unclassified	**unclassified**	**unclassified**	**UU**	**18**	

Standard Form 298 (Rev. 8-98)
Prescribed by ANSI Std Z39-18

INTRODUCTION

As the high performance turbine engine technologies advance, the turbine inlet temperature is raised to higher levels to achieve higher thermal efficiency. Current material technologies require film cooling to protect the turbine airfoils from the hot gas stream, especially the leading edge due to its exposure to the highest temperatures. Minimizing the amount of coolant used in the film cooling requires consideration of techniques to extend the area of film coverage such as the injection angle and the injection hole pitch. Extending the coolant to cover more spanwise and streamwise area by reducing the injection angle and adjusting the blowing ratio, the hole pitch may be increased thus reducing the number of required film holes. This can also increase the strength of the airfoil again due to reduction in the number of film holes.

In the past, many leading edge film cooling studies have used larger injection angles (30º - 35º) and smaller hole pitch (3 - 4 injection hole diameters). Mick and Mayle (1988) performed tests using a blunt body with a circular leading edge and a flat afterbody to study the detailed film effectiveness and heat transfer coefficients for secondary air injection through two rows of holes into the stagnation region of an incident mainstream flow. The holes in each row were spaced four hole diameters apart and were angled 30º to the surface in the spanwise direction. At a low mainstream turbulence they found that large spanwise variations exist in both film effectiveness and heat transfer coefficient. They also reported that the highest values of film effectiveness and heat transfer coefficient do not correspond to the same location. Mehendale and Han (1992) and Ou et al. (1992) used a similar test model as that of Mick and Mayle (1988) to study the effect of the high mainstream turbulence on leading edge film cooling and heat transfer at a Reynolds number of 100,000. They also used a spanwise injection angle of 30º but a hole pitch of three hole diameters. They found that the film effectiveness for a blowing ratio of 0.4 is significantly reduced by high mainstream turbulence and that the heat transfer coefficient for a blowing ratio of 0.8 increases with increasing mainstream turbulence, but the effect is not consistent for blowing ratios of 0.4 and 1.2. They also pointed out that the mainstream turbulence adversely affects the film effectiveness for a blowing ratio of 0.4 but the effect is reduced for blowing ratios of 0.8 and 1.2. The heat transfer coefficient increases with mainstream turbulence levels for blowing ratios of 0.4 and 0.8 but the effect is not consistent for the blowing ratio of 1.2. Ekkad et al. (1995) studied the effect of free stream turbulence on the detailed distributions of film effectiveness and heat transfer coefficient on a cylindrical leading edge model using a transient liquid crystal image method. Again, an injection angle of 30º and a pitch of four hole diameters were used in this study. They found that the heat transfer coefficient increases with an increased blowing ratio but the film effectiveness reaches a peak value at a blowing ratio of 0.4. Their results also show that higher mainstream turbulence reduces the effectiveness for lower blowing ratios but the effect diminishes at higher blowing ratios.

This investigation considers a blade film angle of 20º and a pitch to hole diameter ratio of 7.86 to extend the film coverage over the larger film angles and smaller pitch film holes. Karni and Goldstein (1990) investigated a single row of 20º film holes with a P/d of 5.98 on a cylinder which was rotated to 0º, 7º, 10º, and 30º for blowing ratios of 0.5 to 2.0 using a naphthalene mass sublimation technique to determine the local heat transfer coefficient distribution. Measurements for a similar geometry to the one investigated in this study have been reported by Cruse et al. (1997). Cruse investigated a density ratio of 1.8 with a half plane simulation of the leading edge. An infrared technique was used by Cruse to measure the surface temperature distribution for the film effectiveness and a constant heat flux surface was used to obtain the heat transfer coefficient. Computations for the Cruse geometry have been preformed and reported by Martin and Thole (1997), Thakur et al. (1997), Chernobrovkin and Lakshminarayana (1999), and Lin et al. (1997). The comparisons of the computations with the experiment showed good agreement with film effectiveness but differences in the heat transfer coefficient. Chernobrovkin in their computational work has observed the turbulence length scale has such an effect on the computation that it is impractical to attempt a calculation at Tu=20%. To improve the measurement accuracy of the heat transfer coefficient Yuki et al. (1998) investigated the density ratio of 1.1 for the same experiment but without a direct determination of the film effectiveness for all cases. In the Yuki experiment, the film holes were found to locally distort the electric field generated in the constant heat flux surface which in turn resulted in distortion in the local heat transfer coefficient. Mick and Mayle (1988) noticed the same problem and applied a correction to determine the local heat flux. Yuki presents the heat transfer coefficients as a ratio of the cooled to the uncooled value to remove the distortion effect. Significant increases in the heat transfer coefficients with cooling observed by Cruse, Yuki, and the earlier experiments are of course a significant concern to accurately determine the net heat load to the turbine airfoils.

The transient LC method employed in this effort provides both the film cooling coefficient and the heat transfer coefficient from two sets of measurements on the same configuration with the same thermal boundary conditions which are solved simultaneously. The effects of large values of curvature, pressure gradient, combined with high freestream turbulence at a density ratio of 1.0 are the subjects of this investigation. Two turbulence levels, two Reynolds numbers,

and four blowing ratios are investigated and the resulting heat transfer coefficient (in terms of Frössling number, $Nu/Re^{1/2}$) and the film cooling effectiveness reported.

DESCRIPTION OF THE EXPERIMENTAL FACILITY

The facility shown schematically in Figure 1 consists of a 76.2 cm diameter settling chamber with a 30.5 cm diameter solenoid valve to switch the primary temperature controlled flow from a bypass loop to the test loop. A secondary temperature controlled turbulence flow loop and a third temperature controlled film flow (coolant flow) loop with manual valves complete the flow path. All temperature controlled loops are capable of both heating and cooling. The test article with a height of 36.4 cm is a full half cylinder joined by a flat afterbody. There are three rows of film holes located respectively at the stagnation line and ±21.5º from the stagnation line. Each film hole is staggered with respect to the adjacent row and spanwise spaced 7.86 hole diameters apart. The holes are angled 20º and 90º to surface in the spanwise and streamwise directions. The hole to leading edge diameter ratio is 0.054 and the hole length to hole diameter ratio is 11.69. Nine locations of hot wire traverse stations for flow profile measurements are provided on the top wall.

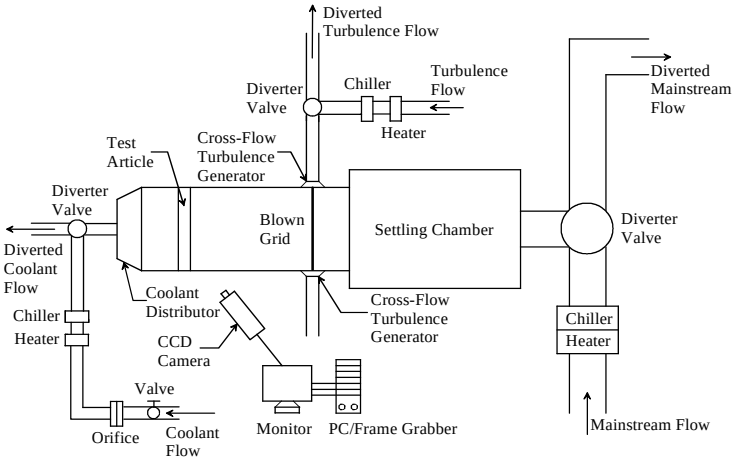

Figure 1. Schematic of Test Facility

The turbulence generator consists of a blown grid plus jets in cross flow to achieve high turbulence intensity and uniform velocity and turbulence profiles over the test section. The blown grid and the cross-flow jet are in the same plane which is located at 118.9 cm upstream of the stagnation line of the test article location (x/b=74.9). Typical velocity profiles show uniformity of 1 to 2% over the film measurement area at both low (about 1%) and high turbulence (about 20%) levels. The midspan centerline velocity and turbulence intensity distributions are shown in Figure 2. The midspan centerline

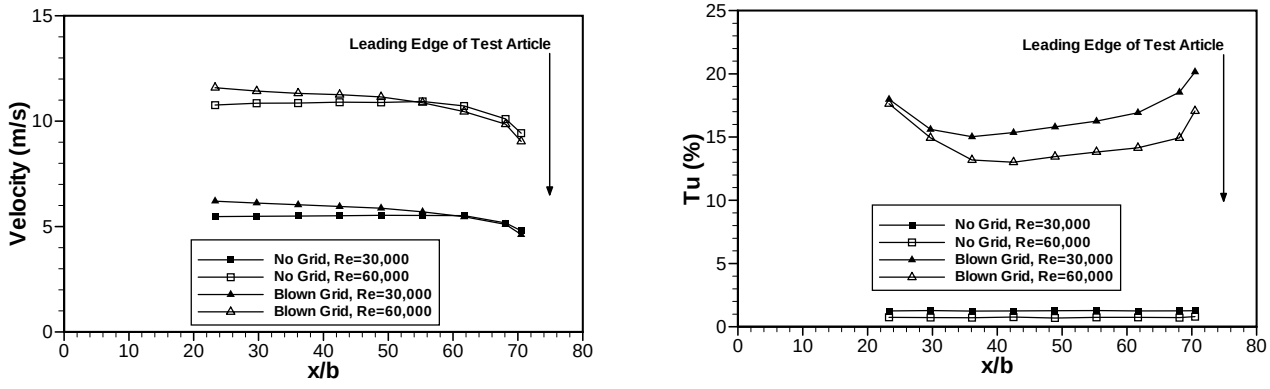

Figure 2. Centerline Velocity and Turbulence Intensity Distributions

velocities show similar trends at both Reynolds numbers. The blown grid initially has higher velocity than the no grid case. This is probably due to the nonuniform mixing between the mainstream flow and the strong jets from the blown grid and the cross flow turbulence generator. As the mixing flow continues downstream, the difference between the velocities reduces gradually until it is within 4% at the location of 6.99 cm upstream of the stagnation. The blown grid turbulence initially decays with x just as a traditional grid until x/b=36.1, where the turbulence starts to increase slightly. As the test article is approached, an increase in turbulence occurs due to the turning of the flow which reduces the axial measured component of velocity. Integral turbulence scales measured by correlation are typically the order of 3 cm (Λ/d = 6.3) at the test article for the high turbulence conditions.

INSTRUMENTATION AND CALIBRATION

A transient technique is employed to measure surface temperature using a wide band liquid crystal (LC). A steady state hue calibration is initially carried out on a flat sample of the batch of liquid crystal used on the test article. The initial LC hue calibration is against a linear array of 19 thermocouples on a water-cooled and heated Aluminum block which provides a linear distribution of temperature to calibrate the wavelength or hue against temperature. The liquid crystal used in the present study is BM/R38C5W/C17-10. The temperature calibration for this particular liquid crystal is 38.3ºC, 39.1ºC and 43.8ºC for the red, green and blue hues, respectively. A second calibration is superimposed upon the original LC calibration to account for the test article different illumination angles, camera view angle, and the curvature of the model. This calibration is accomplished by an in place measurement on the test article. A 2.54 cm wide by .05 mm thick stainless steel foil, constant heat flux surface, with 8 thermocouples distributed around a 90 degree segment is located on the model below the film cooling holes. This calibration strip is also coated with the LC to provide a direct in place LC calibration. A Sony XC-003 three-chip color CCD camera is used to acquire and transfer images. The data which is presented was acquired with a hue system which was originally developed by Farina and Moffat (1994) at Stanford University utilizing a Matrox frame grabber. A constant heat flux surface on the model has also been used to check the value of heat transfer coefficient in the stagnation region. Figure 3 shows the measured leading edge Frössling number distribution for the cylinder without film holes at the Re = 30,000, 60,000, and low turbulence conditions. Also superimposed on Figure 3 are the experimental data for Re=100,000 from Mick and Mayle (1988) and Re=71,000 from Giedt (1949). The Frössling numbers show reasonable agreement although the Reynolds numbers are all different and turbulence levels also vary slightly.

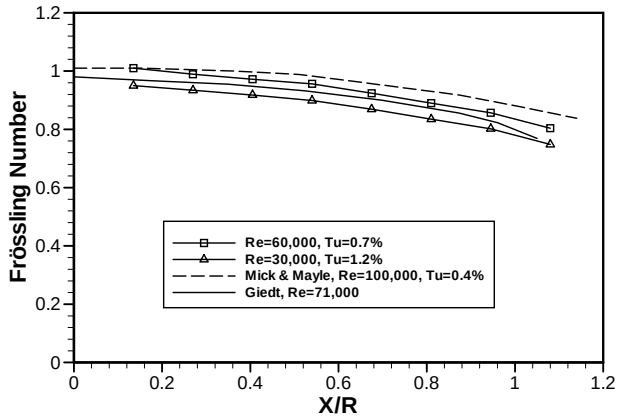

Figure 3. Frössling Number Distribution on the Leading Edge Model Without Film Holes

MEASUREMENT OF THE DISCHARGE COEFFICIENTS

Several calculations of the heat transfer coefficient and the film cooling effectiveness for a very similar geometry have been carried out by Chernobrovkin et al., 1999, Lin et al., 1997, Martin et al., 1997, and Thakur et al., 1997. The discharge coefficient is sensitive to the entrance radius, entrance and exit cross flow and film hole l/d, Reynolds numbers, and possibly the turbulence and turbulence scales as well. The computations all began on the back side of the film

cooling holes so most of the traditional effects were included in the calculations but not in the initial experimental measurements.

$$\rho U_f A\big|_{\text{total orifice 3 rows}} = \left(C_{D,0^\circ}\rho_{0^\circ}U_{0^\circ}A_{0^\circ} + C_{D,21.5^\circ}\rho_{21.5^\circ}U_{21.5^\circ}A_{21.5^\circ}\right)\Big|_{\text{ideal}} \quad (1)$$

The effect for a given orifice measured blowing ratio is to have actual blowing ratios that are higher at the 21.5º row than at the stagnation row. The recent literature does not provide specific measurements for skew film holes. Available experimental and calculated discharge coefficients have a range of values from 0.3 to 0.8 (Burd and Simon, 1998). Since the blowing ratio is a critical parameter in comparison of experimental and computational data, direct measurements were undertaken to minimize this uncertainty in the comparisons. C_D is given by the ratio of the actual flow to the value calculated by the isentropic expansion for the pressures and temperatures involved.

The coolant flow was supplied from the back side of the test model, as shown in Figure 1. The coolant flow then passed through flow conditioning elements for uniform distribution with no internal cross flow velocity. The actual total flow rates ($\dot{m}_f$) were measured by an orifice plate meter for both cases at the stagnation and 21.5º rows. When the measurement was made for the stagnation row, all the film holes at the ±21.5º row were blocked by tapes on the outer surface of the model (as suggested by Rowburg et al., 1998). A similar procedure was taken for the flow rate measurement at the ±21.5º row.

$$C_D = \frac{\dot{m}_f}{\dot{m}_{id}} = \frac{\dot{m}_f}{A\left(\frac{p_e}{p_t}\right)^{\frac{1}{\gamma}} \frac{p_t}{\sqrt{RT_t}} \sqrt{\frac{2\gamma}{\gamma-1}\left[1-\left(\frac{p_e}{p_t}\right)^{\frac{\gamma-1}{\gamma}}\right]}} \quad (2)$$

Static pressures at the hole exit (p_e) were measured by taps located at 0º, and 21.5º on a model without film holes. The total film cooling plenum pressure (p_t) and total temperature (T_t) were measured two hole diameters from the back side of the film holes. Free stream conditions were used as the reference for setting the blowing ratio. Free stream velocities were measured five cylinder diameters upstream of the cylinder on the centerline of the test section with a pitot tube probe. The stagnation temperature was measured at the same location of velocity measurement and at the exit of the section.

The measured discharge coefficients for the two film row locations by Equation (2) for four blowing ratios at Re=60,000 and 30,000 are shown in Table 1. The computed C_D at the stagnation row for a blowing ratio of 2.0 at a Re ≈ 60,000 (Thole, 2000), was found to be 0.6 for a similar geometry.

Table 1. Discharge Coefficients at Re = 60,000 and 30,000

Orifice Blowing Ratio	C_D at 0º 60,000 / 30,000	C_D at 21.5º 60,000 / 30,000
1.0	0.688 / 0.388	0.537 / 0.466
1.5	0.658 / 0.483	0.561 / 0.494
2.0	0.665 / 0.515	0.564 / 0.506
2.5	0.619 / 0.538	0.590 / 0.520

The exit velocity profile for very short holes, l/d < 3, is Volcano like with ± 20%U_∞ excursions about U_∞, (Rivir and Goginnini, 1996) while for long l/d holes > 7 the profile flattens out within a few % of U_∞ (Burd and Simon, 1998). The l/d of film holes of the present study is 11.69. Since the Re_d of the film hole flows is between 1,605 and 8035 the profile would be expected to be laminar at the blowing ratio of 1.0, transitional between 1.0 and 1.5 and turbulent for 2.0 and 2.5 flows for Re=30,000 and turbulent for all of the Re=60,000 flows. The average of a laminar profile is given by 0.5 U_{max}, as reflected in the low discharge coefficient for the blowing ratio of 1.0 at Re=30,000. Since the measured C_D's are approximately constant for all blowing ratios at the same row at Re=60,000, the turbulent profile would be approximately given by (Bird, et al., 1966)

$$U / U_{max} \cong (1 - r/R)^{1/7} \quad (3)$$

which gives upon integration

$$U_{avg} \cong 0.869\, U_{max} \tag{4}$$

The total flow for the combined three film rows was measured by orifice plate meter. The orifice flow was compared against the film hole measured values for U_{max} and U_{avg} using Equations (4) and (5) assuming no changes in the densities.

$$U_f\, 3A = U_{f,0^\circ} A + U_{f,21.5^\circ}\, 2A \tag{5}$$

The velocities for the individual holes were measured with a miniature hot wire at the film hole centerlines. While the relative hot wire values are very accurate the absolute values are only good to 15% in this application, due to difficulties in accurately positioning the hot wire in the film hole. Film hole velocities were found to be uniform to 0.1% to 1% at 0º row and 0.3% to 4% at 21.5º row. The calculated average flows agree with the orifice flow within +2.2%, -1.8%, and -6.1% using U_{max}, and –8%, -12%, and –15% using U_{avg} for the blowing ratios of 1.0, 1,5, and 2.0, respectively.

Table 2. Individual Row Blowing Ratios at Re = 60,000

Orifice Blowing Ratio	0° Row Blowing Ratio (U_{max})	21.5° Row Blowing Ratio (U_{max})
1.0	0.93 (10.36)	1.00 (11.10)
1.5	1.48 (16.39)	1.55 (17.23)
2.0	2.03 (22.58)	2.17 (24.05)

The calculated blowing ratios, based on U_{max}, in Table 2 show a nominal 6% higher than velocity or blowing ratio at 21.5º row compared to 0º row.

THEORY OF THE TRANSIENT LIQUID CRYSTAL TECHNIQUE

Transient heat transfer in a solid substrate coated with liquid crystal, which is suddenly exposed to a convective fluid at temperature T_m, is governed by transient heat diffusion equation. Under the assumptions of one-dimensional heat conduction (e.g., in the x direction) and without film injection, the local heat transfer coefficient, h, can be obtained by solving the following governing equation with the prescribed boundary conditions.

$$k\frac{\partial^2 T}{\partial x^2} = \rho c_p \frac{\partial T}{\partial t} \tag{6}$$

where k is the thermal conductivity of solid, T the surface temperature, x the coordinate perpendicular to the surface (+ towards the inside of the solid), ρ the density of the solid, c_p the specific heat of the solid, and t the time.

$$T(x,0) = T_i \tag{7}$$

$$-k\frac{\partial T}{\partial x}\Big|_{x=0} = h\left[T_m - T(0,t)\right] \tag{8}$$

$$T(\infty,t) = T_i \tag{9}$$

The solution to Equation (6) can be obtained in the form of the dimensionless temperature at the convective boundary surface (i.e., x=0) as follows.

$$\frac{T_w - T_i}{T_m - T_i} = 1 - \exp\left[\frac{h^2\alpha t}{k^2}\right] erfc\left[\frac{h\sqrt{\alpha t}}{k}\right] \tag{10}$$

where T_w is surface temperature, T_i the initial temperature, T_m the convective fluid temperature, and the thermal diffusivity of the solid.

For the situation with a single convecting fluid at temperature T_m, for example, a solid test surface coated with liquid crystal without film injection, the local heat transfer coefficient (h) can be obtained from Equation (10) by knowing the initial temperature (T_i) of the test surface and the fluid flow temperature (T_m) and measuring the liquid crystal coated surface temperature indicated by the color display (T_w) at time (t). In the film cooling application over a surface, however, there are three temperatures involved: the mainstream temperature T_m, the coolant temperature T_c, and the wall temperature T_w. For the film cooling case, the mainstream temperature T_m in (10) must be replaced by a film temperature T_f, which is the mixed temperature between the mainstream and coolant temperatures and governs the convection on the liquid crystal coated surface. (10) may be rewritten as:

$$\frac{T_w - T_i}{T_f - T_i} = 1 - \exp\left[\frac{h^2 \alpha t}{k^2}\right] erfc\left[\frac{h\sqrt{\alpha t}}{k}\right] \tag{11}$$

to find the unknown T_f in terms of known quantities T_m and T_c, a dimensionless temperature is defined as the film cooling effectiveness (η).Vedula and Metzger (1991) first introduced a technique to obtain the film effectiveness and heat transfer

$$\eta = \frac{T_f - T_m}{T_c - T_m}; \quad \text{or} \quad T_f = \eta\,(T_c - T_m) + T_m = \eta\, T_c + (1-\eta) T_m \tag{12}$$

coefficient involving in a three temperature, film cooling problem. Based on this approach, two separate but closely related tests are performed. In the first (cold) test, the mainstream is heated to the desired value depending on the liquid crystal in use while the coolant is slightly heated. In the second (hot) test, the mainstream and coolant are respectively heated to desired temperatures. In both tests the test article remains at room temperature. In the experiments, the true step changes in the applied fluid temperatures (both mainstream and coolant) are usually not possible and actually change with time. The actual time-dependent fluid temperature changes can be accounted for by modifying the equations using superposition and Duhamel's theorem with the fluid temperatures replaced by a series of steps. The solution of Equation (11) is represented as:

$$T_w - T_i = \sum_{j=1}^{N} U(t - \tau_j)(T_f - T_i)_j \tag{13}$$

$$U(t-\tau_j) = 1 - \exp\left[\frac{h^2}{k^2}\alpha(t-\tau_j)\right] erfc\left[\frac{h}{k}\sqrt{\alpha(t-\tau_j)}\right] \tag{14}$$

where T_f is time varying and unknown but related to the time variation in T_m and T_c and to the film cooling effectiveness. Substituting T_f from Equation (12) into Equation (13) and rearranging the equation, the final forms related to the respective first and second transient tests are:

$$T_w - T_{i1} = \sum_{j=1}^{N_1} U(t-\tau_j)\left[(1-\eta)(T_{m1} - T_{i1}) + \eta(T_{c1} - T_{i1})\right]_j \tag{15}$$

$$T_w - T_{i2} = \sum_{j=1}^{N_2} U(t-\tau_j)\left[(1-\eta)(T_{m2} - T_{i2}) + \eta(T_{c2} - T_{i2})\right]_j \tag{16}$$

where N_1 and N_2 are the numbers of time steps to reach the detected temperature for the first and second transient tests, respectively. The two equations (15 and 16) are solved to obtained the two unknowns, h and η for each pixel in the measurement region of interest.

MEASUREMENTS OF FILM COOLING EFFECTIVENESS AND HEAT TRANSFER COEFFICIENT

The coolant flow temperature is measured by a thermocouple in the coolant chamber adjacent to a film hole. Air is used as film flow which results in a nominal density ratio of one, although the actual value varies between 1.02 and 1.06 during the transient test. The mainstream temperature is measured by a thermocouple in the plane of the stagnation line of the test article. The initial temperature of the test article is measured by a thermocouple attached to the outer surface on the flat afterbody as shown in Figure 4. Another thermocouple attached on the inner surface of the coolant chamber is used to check the initial temperature and assure no gradient of temperature across the wall of the test article.

All the flows involved are initially diverted away from the test article by bypass loops. The flow temperatures are heated to the desired values and reach steady state during this period. A transient test is initiated by switching valves simultaneously with the test loop to force the mainstream flow, film flow and turbulence flow over the test article. The initiation of the transient test triggers a data acquisition system to record the mainstream flow and coolant flow temperatures. Two independent tests are performed for each case. The data will be reduced as described in the preceding section.

The leading edge is simulated by a full half cylinder joined by a flat afterbody of 20.32 cm in length. The test article is 1.91 cm thick Plexiglass throughout in order to provide the required infinite wall boundary condition. The measurement domain on the test surface is divided into 81 pixels streamwise and 138 pixels spanwise which cover two repeated hole cycles. The CCD camera records the images, converting them into an array of temperatures. A Fortran program is used to solve simultaneously for the film effectiveness and heat transfer coefficient from Equations (15) and (16) at each pixel using the data from two temperature sets. The time for each pixel to reach a particular wave length or hue, a green hue in this case, is computed for each frame. The actual pixel representation on the surface or the local spatial resolution of h and η of the test article is about 0.6 mm. A liquid crystal image of the cylinder surface is shown in Figure 4 for the Re=30,000, M=1.5, and Tu=1.2% case.

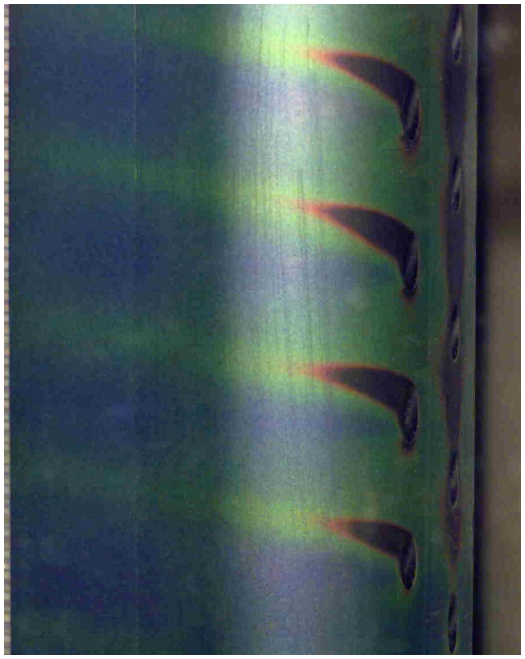

Figure 4. Liquid Crystal Image for Re = 30,000, M = 1.5, Tu = 1. 2%

The major uncertainty in the transient liquid crystal measurement is contributed by the measured time for the each pixel location to reach the particular color (temperature). The expected maximum error in time for the measured color change is ±0.5 sec. The error associated with color calibration against temperature using thermocouples is estimated at

±0.25ºC. Other uncertainty contributions include thermocouple measurements for mainstream and coolant temperatures, flow measurement to determine Reynolds number, blowing ratio and turbulence intensity, and the test surface properties such as thermal conductivity, and thermal diffusivity. Taking these factors into account gives an uncertainty in h of 8% based on the odds of 20 to 1 and the method introduced by Kline and McClintock (1953). Since the heat transfer coefficient is first computed from the Equations (15) and (16), the uncertainty of h is also involved in that of the Frössling number and film effectiveness. The resulting uncertainty of Frössling number is estimated to be 8.1%. The uncertainty in the film cooling effectiveness is estimated to be 10.2%.

RESULTS AND DISCUSSIONS

The film flow rates are measured with an orifice plate meter. Individual periodic hole flow does not assure that the spatial flow is periodic. The LC measurements indeed indicate the flow accumulates from the lower spanwise film injection holes over the upper holes. The detailed film effectiveness distribution of the measurement domain is shown in Figure 5 for the Re=60,000, M=2.0, Tu=0.7% case. The film effectiveness contours of nominally 0.40 on the stagnation row increase at an angle 6° as a result of the increasing spanwise flow.

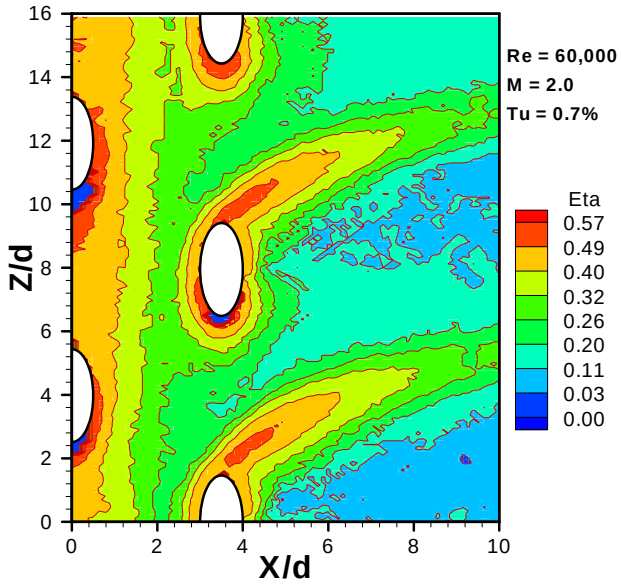

Figure 5. Detailed Film Effectiveness Distribution of Entire Measurement Domain for Re=60,000, M=2.0,Tu=0.7%

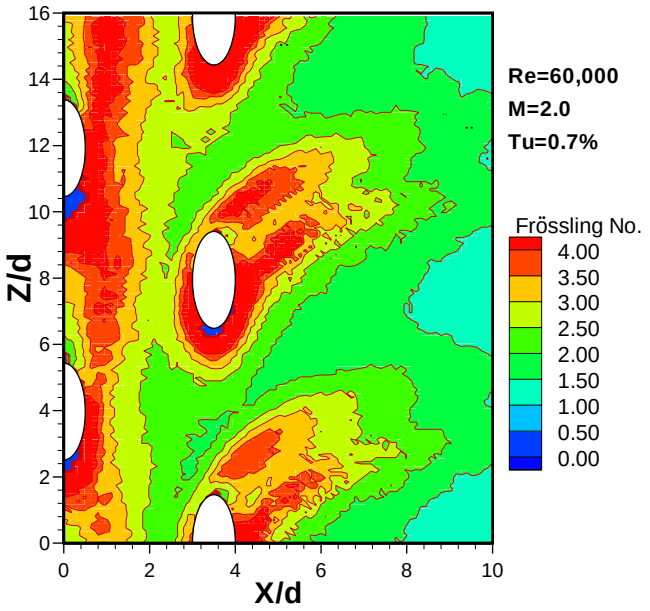

Figure 6. Detailed Frössling Number Distribution of Entire Measurement Domain for Re=60,000, M=2.0, Tu=0.7%

Figure 6 shows the detailed Frössling number distribution of the measurement domain. The Frössling number distribution of constant contours likewise shows a spanwise flow accumulation. It is noted that the contours of the Frössling number are different from those of the film effectiveness. This agrees with the finding by Mick and Mayle (1988) that the highest values of film effectiveness and heat transfer coefficient do not correspond to the same location. This finding was also confirmed by Yuki et al. (1998). The measurement domain covers two repeated hole cycles to check the periodicity. After the 21.5º row Figures 5 and 6 indicate uniform periodicity.

The detailed distributions of film effectiveness and Frössling number are averaged in the spanwise direction. The liquid crystal data within the film holes is biased because it is not on the test surface. The computed spanwise averages have distorted the true values of heat transfer coefficient and film effectiveness at the hole location. The spanwise averaged film effectiveness and Frössling numbers between film holes are therefore excluded from our plots as presented in the following figures.

Effect of Turbulence Intensity

Normally it is expected that high free stream turbulence spreads the film laterally and vertically resulting in a lower spanwise averaged film effectiveness. Figure 7 illustrates the film effectiveness for Re=30,000 at two different turbulence levels for the four blowing ratios. The high free stream turbulence reduces the film effectiveness for all blowing ratios. Between the rows of film holes there is a 61% to 20% reduction in film effectiveness. After the 21.5º row the attenuation ranges from 46% to 21% at X/d=8. The free stream turbulence has a more significant effect at M=1.0 and M=1.5 than M=2.0 and M=2.5.

Figure 8 compares the film effectiveness for Re=60,000 at two different turbulence levels for the four blowing ratios. Unlike the Re=30,000 case, the high free stream turbulence does not always reduce the film effectiveness. Between the rows of film holes there is a reduction in film effectiveness due to the free stream turbulence. For the region downstream of the 21.5º row, with the exception for M=1.5, high free turbulence results in increases in the film effectiveness for M=1.0, 2.0, and 2.5. This is because the high free stream turbulence causes the coolant flow from the 21.5º row to spread more in the spanwise direction creating larger uniform film coverage which averages to a higher film effectiveness. If a more spanwise spread results in smaller film coverage, the resulting film effectiveness is lower as illustrated in Figure 7 for the Re=30,000 high free stream turbulence cases.

Figure 9 shows the Frössling number for Re=30,000 at two different turbulence levels for the four blowing ratios. The high free stream turbulence consistently causes less uniform and lower local Frössling number distributions on the region between two rows of film holes for all blowing ratios. The coolant jets are also depressed by the high mainstream turbulence downstream of 21.5º row. Therefore the film coverage area is reduced and results in lower Frössling numbers for all blowing ratios. However, the reductions are smaller compared to the film effectiveness cases. The free stream turbulence has a more significant effect in the region between two rows (for example at M=2.5, 17% to 21% vs. 3% to 19%) than the region after the 21.5º row for all blowing ratios.

Figure 10 compares the Frössling number for Re=60,000 at two different turbulence levels for the four blowing ratios. Like the Re=30,000 cases, the less uniform and lower local Frössling number distribution on the region between two rows of film holes due to the high free stream turbulence also exists for Re=60,000 cases. The film coverage area reduction downstream of 21.5º row occurs at M=1.0 and M=1.5 but not for the case at M=2.5. For the M=2.0 case the film effectiveness in Figures 7 and 8 is the highest. Likewise, in Figure 10 the Frössling number is also the highest for the M=2.0 case. This is again because the spanwise spread with high turbulence results in a larger uniform distribution which averages to higher Frössling numbers. The high free stream turbulence reduces the Frössling number up to 30% for all blowing ratios in the region between the two rows of film holes. The effect reduces as blowing ratio increases. The free stream turbulence has a much smaller effect after the 21.5º row for all blowing ratios.

The effect of free stream turbulence on the Frössling number between the stagnation and the 21.5º row is not in the expected direction (Figures 9 and 10) from the measured traditionally observed effect on the film effectiveness (Figures 7 and 8). This is believed to be a result of the strong coupling observed between the rows.

Effect of Blowing Ratio

Figure 11 shows the effect of blowing ratio on the spanwise averaged film effectiveness and Frössling number for Re=30,000 at low turbulence. The Frössling number generally increases as blowing ratio is increased with the exception of the M=2.0 case. The same trends do not follow for the film effectiveness. M=2.0 provides the highest film effectiveness and all film effectiveness distributions collapse together except for M=1.0. The collapsed distributions may suggest a coolant flow lift-off from the test surface.

Figure 12 shows the effect of blowing ratio on the spanwise averaged film effectiveness and Frössling number for Re=30,000 at high turbulence. The high turbulence case shows a stronger blowing ratio effect on the film effectiveness with factors of 2.0 to 2.8 times the M=1.0 case between the rows to 2.1 times at X/d=8. This is compared with 1.2 to 1.6 times between the rows to 1.4 times at X/d =8 of the low turbulence case shown in Figure 11. M=2.0 shows the highest values in both film effectiveness and Frössling number. The blowing ratio has more pronounced effect on film effectiveness than on the Frössling number.

Figure 13 presents the effect of blowing ratio on the spanwise averaged film effectiveness and Frössling number at Re=60,000 and Tu=17.5%. The M=1.0 case provides the lowest film effectiveness as well as Frössling number. M=2.0 provides the highest film effectiveness but also the highest Frössling number. There exist only minor differences in both film effectiveness and Frössling number among M=1.0, 1.5, and 2.5 for $1 < X/d < 3$ and $X/d > 5.8$.

Effect of Reynolds Number

The effect of Reynolds number on the spanwise averaged film effectiveness for high turbulence case at four blowing ratios is presented in Figure 14. As Reynolds number increases, the film effectiveness also increases for all blowing ratios. The trends show agreement with Mehendale and Han (1993). Reynolds number is seen to have a major effect only at the low blowing ratio of M=1.0, with a 55% reduction due to a decrease in Reynolds number both between the rows and after the 21.5º row. The effect diminishes as blowing ratio increases until there is virtually no effect for the M=2.5 case.

Figure 15 presents the effect of Reynolds number on the spanwise averaged Frössling number for high turbulence case at four blowing ratios. The Frössling number increases as Reynolds number increases with an exception for the region between the two rows at M=2.5. Although Frössling number has taken into account the square root of Reynolds number, there still exists an effect of Reynolds number. The variations of Frössling number are 0.5% to 40% between the rows and 1% to 27% after the 21.5º row. The results show the same trends with Mehendale and Han's study, in which the Frössling number increases 19 % after the first row and 21% after the second row for M=0.8 as Reynolds number increases from 25,000 (Tu=8.53%) to 40,000 (Tu=7.59%).

The Blowing Ratio 2.0 Case

In Figure 6 the blowing ratio 2.0 case shows the coolant flow from the bottom hole on the stagnation row merges with that of the 21.5º row and extends over the 21.5º row (see the contour level of 2.50). A similar situation is also observed in Figure 5 (see the contour level of 0.26).

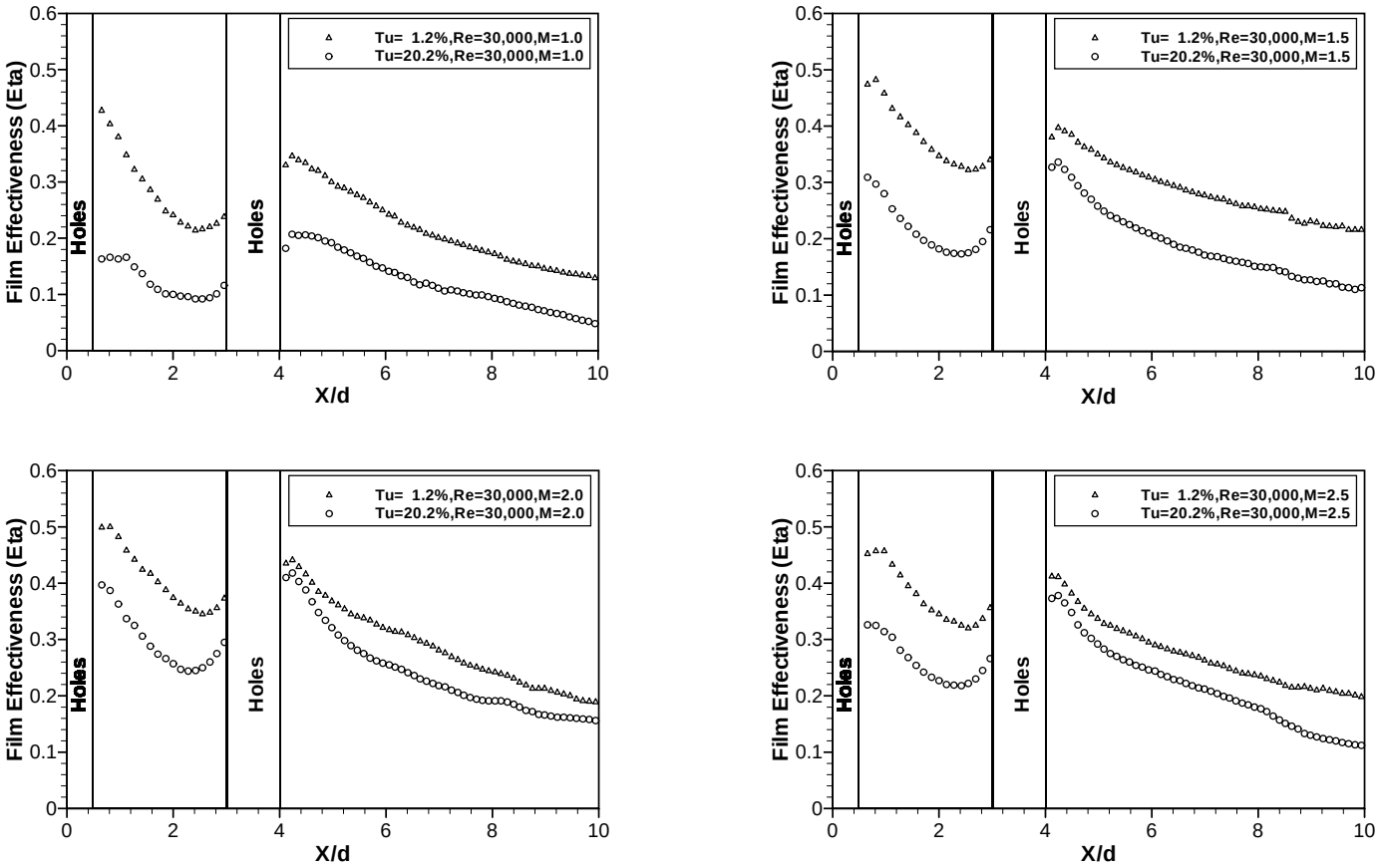

Figure 7. Effect of Turbulence on Spanwise Averaged Film Effectiveness for Re=30,000 at Four Blowing Ratios (M=1.0, 1.5, 2.0, and 2.5)

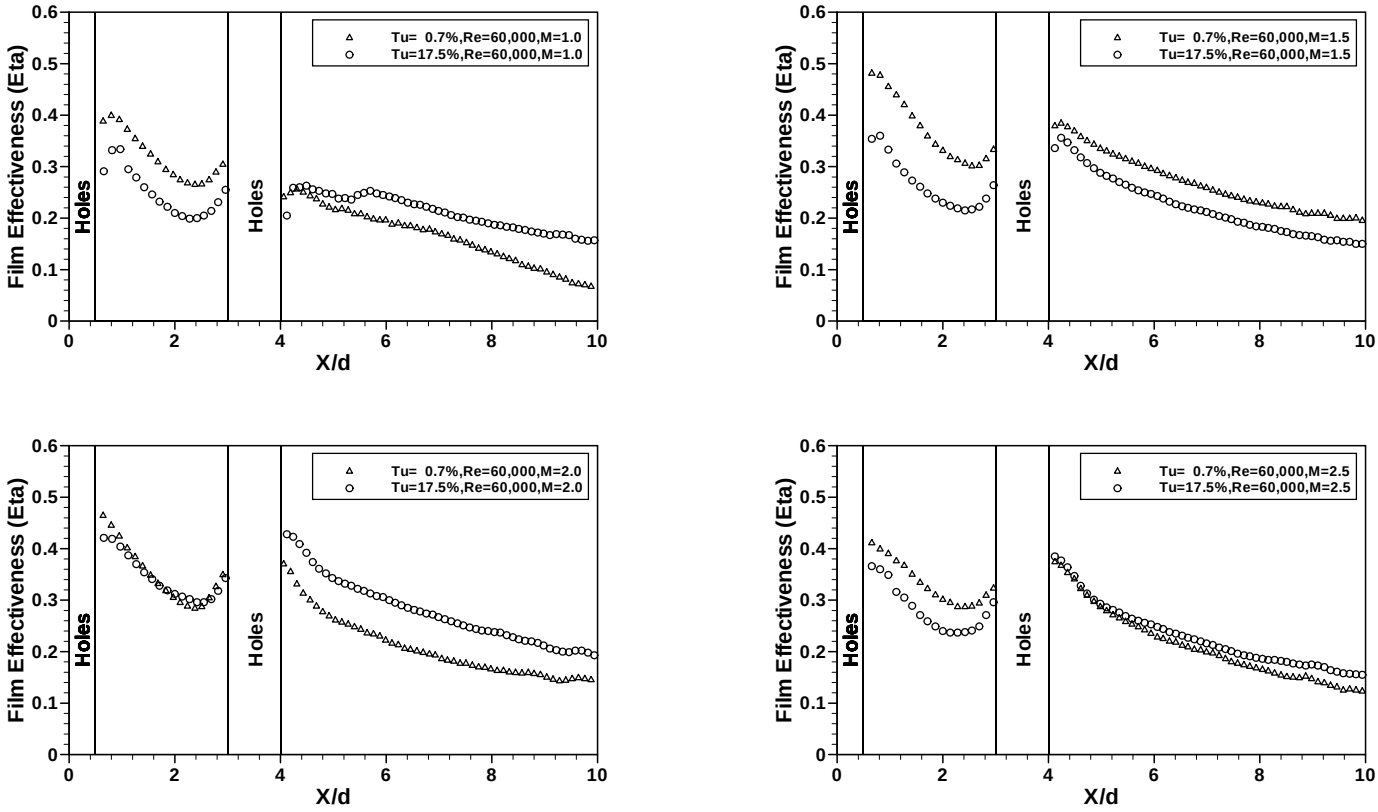

Figure 8. Effect of Turbulence on Spanwise Averaged Film Effectiveness for Re = 60,000 at Four Blowing Ratios (M = 1.0, 1.5, 2.0, and 2.5)

This allows coolant flow to be ingested by the 21.5º film holes to provide improved cooling from the 21.5º row holes. This would suggest that subtle adjustments of the relative positions of the stagnation relative to the 21.5º row and blowing ratio could improve the performance with possibly a smaller cooling flow. Other blowing ratios show interactions of the two film rows as well but the M=2.0 case illustrates the largest effects on the film effectiveness and Frössling number.

Comparison with Other Results

The measured film effectiveness values are consistent with the experiments currently reported in the literature, Cruse et al. (1997) Yuki et al. (1998), and Reiss and Bölcs (1999), considering the differences in the experiments. The differences in the measured h values however remain significant. The parameter $Tu*Re^{0.5}$ has been used by Smith and Kuethe (1966) and VanFossen and Ching (1994) for uncooled stagnation flows with success. The values of $Nu/Re^{0.5}$ normalized by the values from Smith and Kuethe have been plotted against $Tu*Re^{0.5}$ for several experiments in Figure 16a and b after the first row and after the second row of film holes respectively. It is noted that the first and second row of film holes may not be at the same locations. This experiment shows agreement after the second row with Mehendale and Han (1993), the only experiment with a wide range of $Tu*Re^{0.5}$, to better than 16%, with the exception of our M=2.0 case, where strong coupling between the stagnation row and the 21.5º row was observed. The spread in the data at the first row is quite large as shown Figure 16a. After the second row of film holes the spread collapses some but remains sizable. There are however similar slopes to our data, Mehendale and Han (1993), and Reiss and Bölcs (1999) with the Smith and Kuethe parameter of $Tu*Re^{0.5}$. Comparison after second row with Yuki et al. (1998), a very similar experiment to the present one, indicates differences of –49% with Mehendale and Han's data and –56% from our data for h. While there are significant differences in flows, film holes configurations, boundary conditions and measurements techniques, these are not expected to account for the differences observed in h. The error estimates for all these experiments would seem to negate the possibility of the difference to be due simply to measurement errors. We have noted very strong interactions between the two rows of film holes. These interactions may be coupled with other flow and boundary layer parameters.

In the attempt to scale up the experiments to allow improved spatial resolution of the distributions of h and η experimenters are forced to address simulation of a number of parameters such as D/Λ, d/Λ, d/δ, Λ/δ, λ/δ, λ/Λ, and Mach number. These parameters are normally thought to be secondary effects. When these effects are combined with some of the other variables of the problem they may become significant players, particularly in the leading edge problem. The integral (Λ) and micro scales (λ) of turbulence are examples of such a case. VanFossen and Ching (1994) has addressed the integral scale case without film cooling and proposed an empirical relationship with intensity and scale for the Frössling number which has a continual increase in h as the integral scale is decreased. Likewise it was pointed out by Chernobrovkin and Lakshminarayana (1999) that the turbulence scale interaction presents a problem for the computations as well. Since these measurements were taken we have improved both the spatial and temporal resolution by factors of 12 or more. In making spot checks of the data with higher resolution measurements we believe what is presented to be an accurate representation of a data set for this experiment.

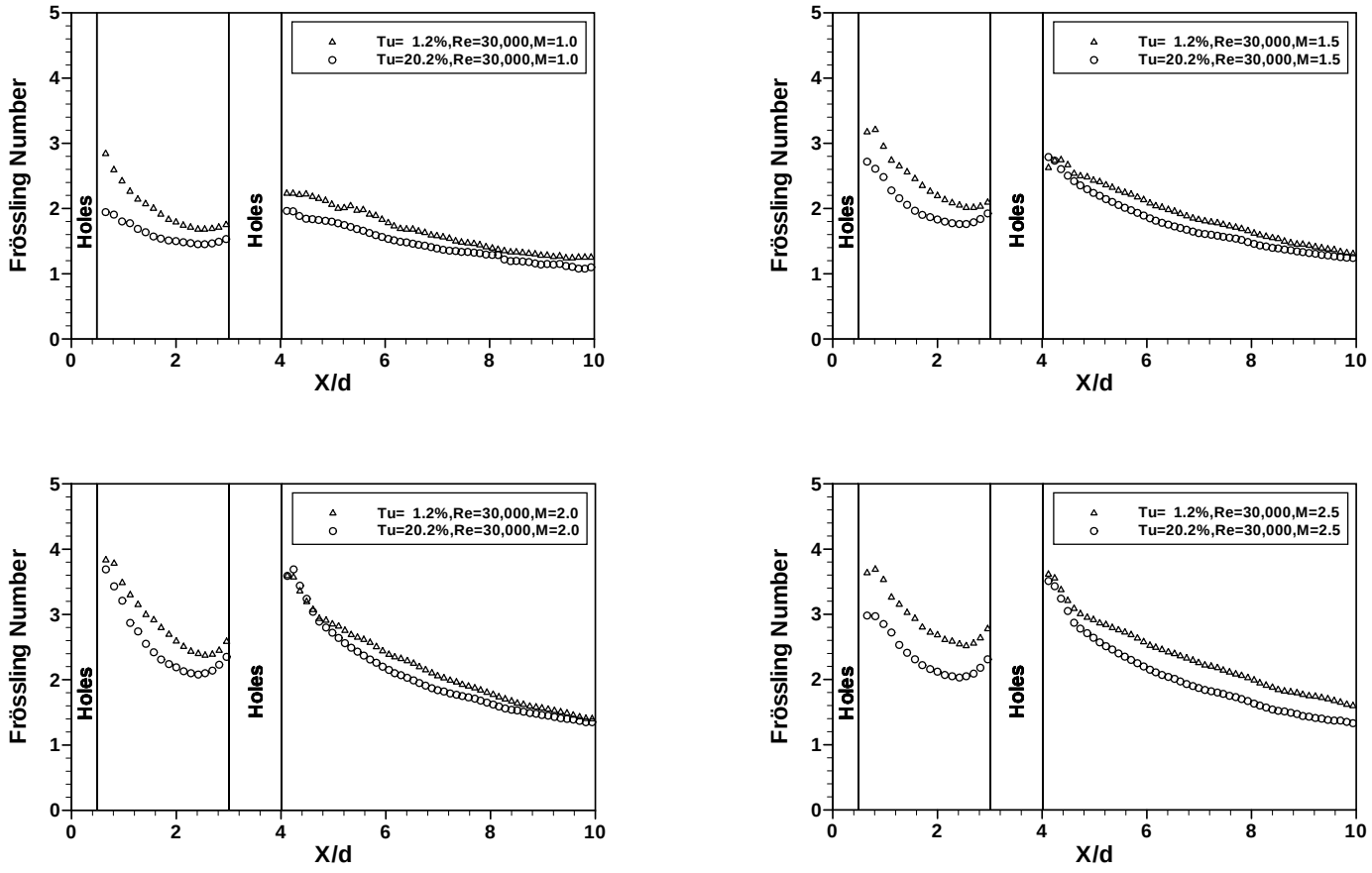

Figure 9. Effect of Turbulence on Spanwise Averaged Frössling Number for Re = 30,000 at Four Blowing Ratios (M=1.0, 1.5, 2.0, and 2.5)

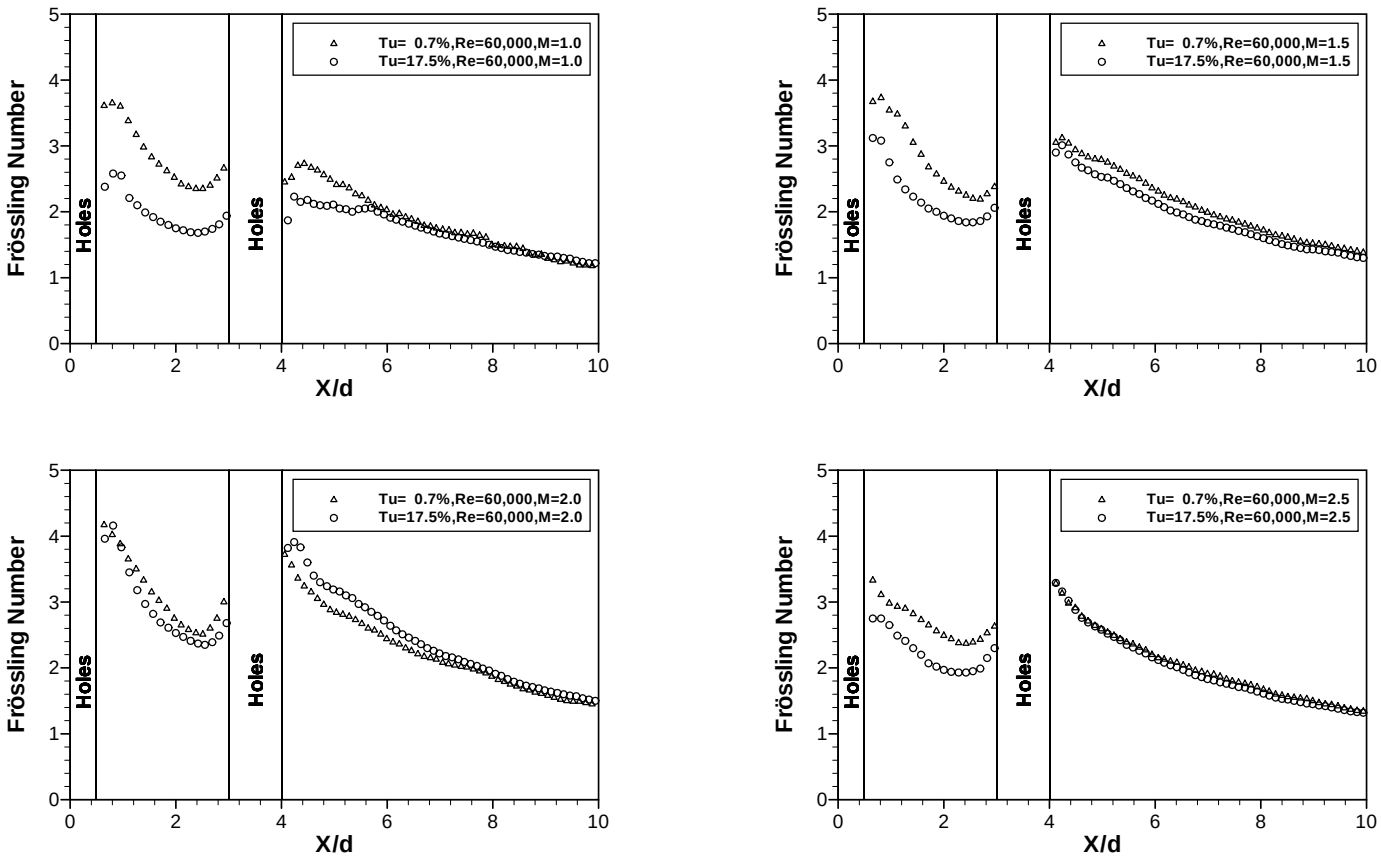

Figure 10. Effect of Turbulence on Spanwise Averaged Frössling Number for Re = 60,000 at Four Blowing Ratios (M = 1.0, 1.5, 2.0, and 2.5)

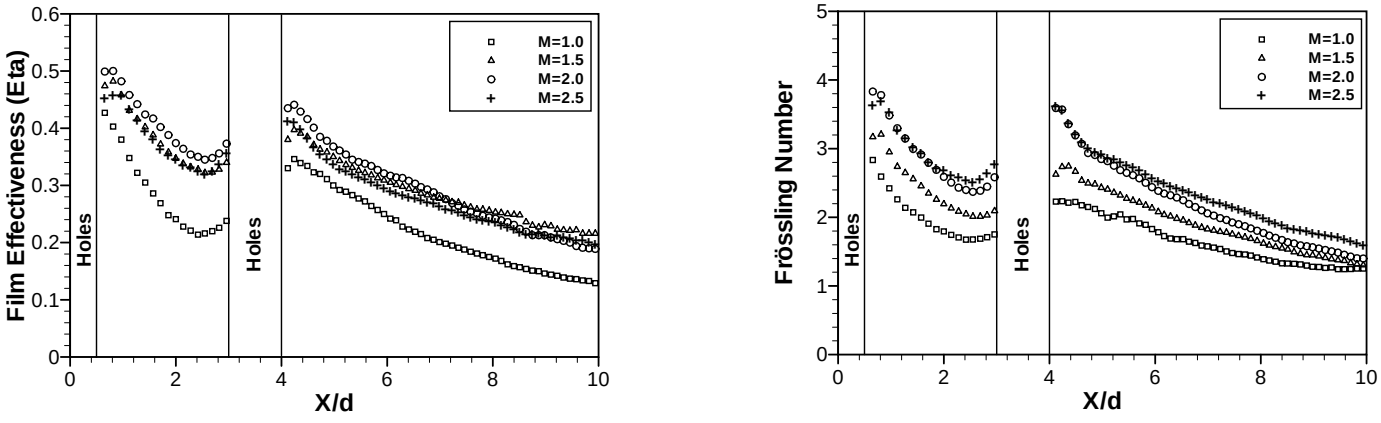

Figure 11. Effect of Blowing Ratio on Spanwise Averaged Film Effectiveness and Frössling Number for Re = 30,000 and Low Turbulence (Tu = 1. 2%)

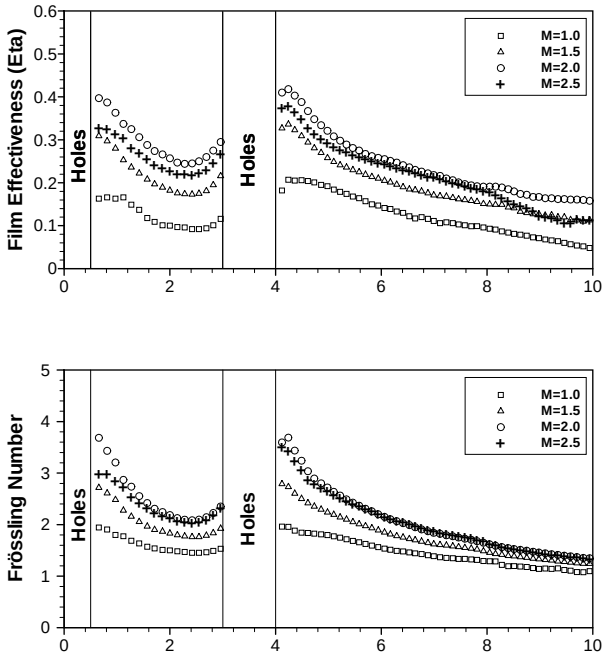

Figure 12. Effect of Blowing Ratio on Spanwise Averaged Film Effectiveness and Frössling Number for Re = 30,000 and HighTurbulence (Tu = 20.2%)

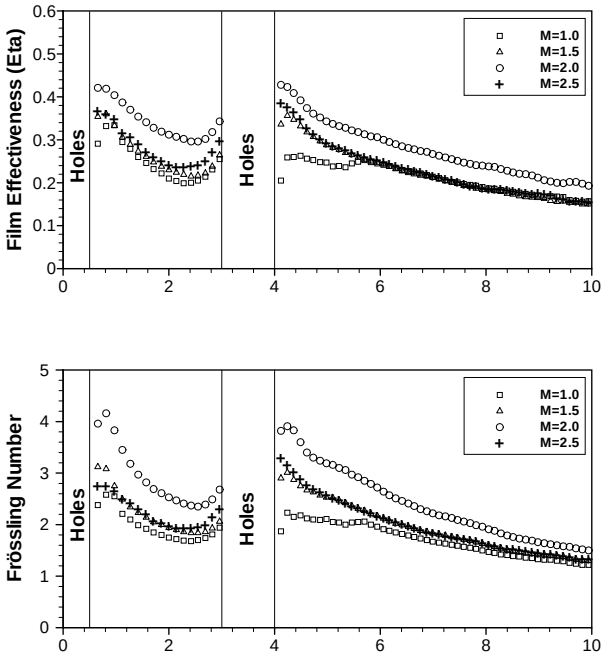

Figure 13. Effect of Blowing Ratio on Spanwise Averaged Film Effectiveness and Frössling Number for Re = 60,000 and High Turbulence (Tu = 17.5%)

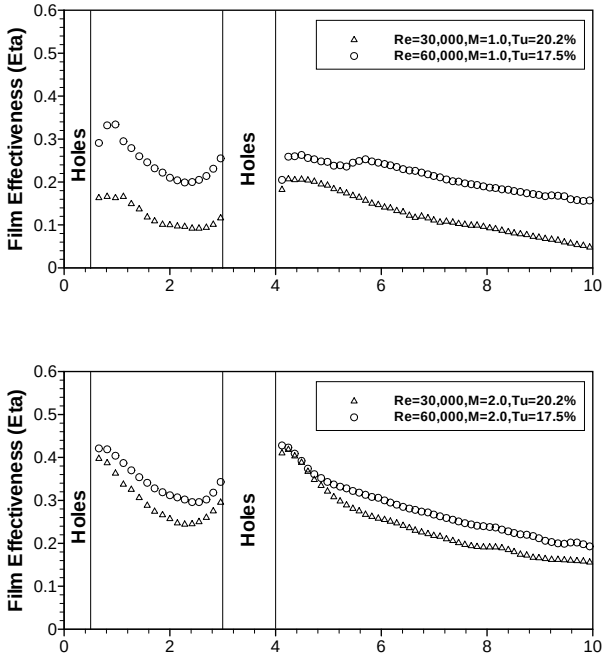

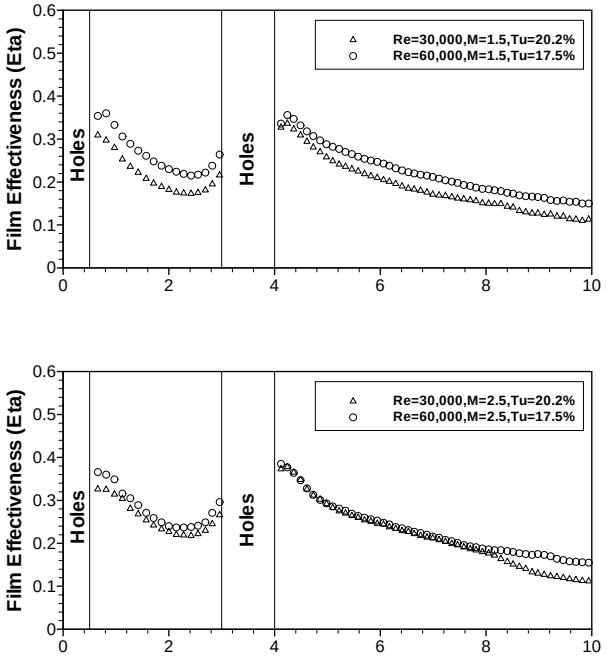

Figure 14. Effect of Reynolds Number on Spanwise Averaged Film Effectiveness for High Turbulence at Four Blowing Ratios (M = 1.0, 1.5, 2.0, and 2.5)

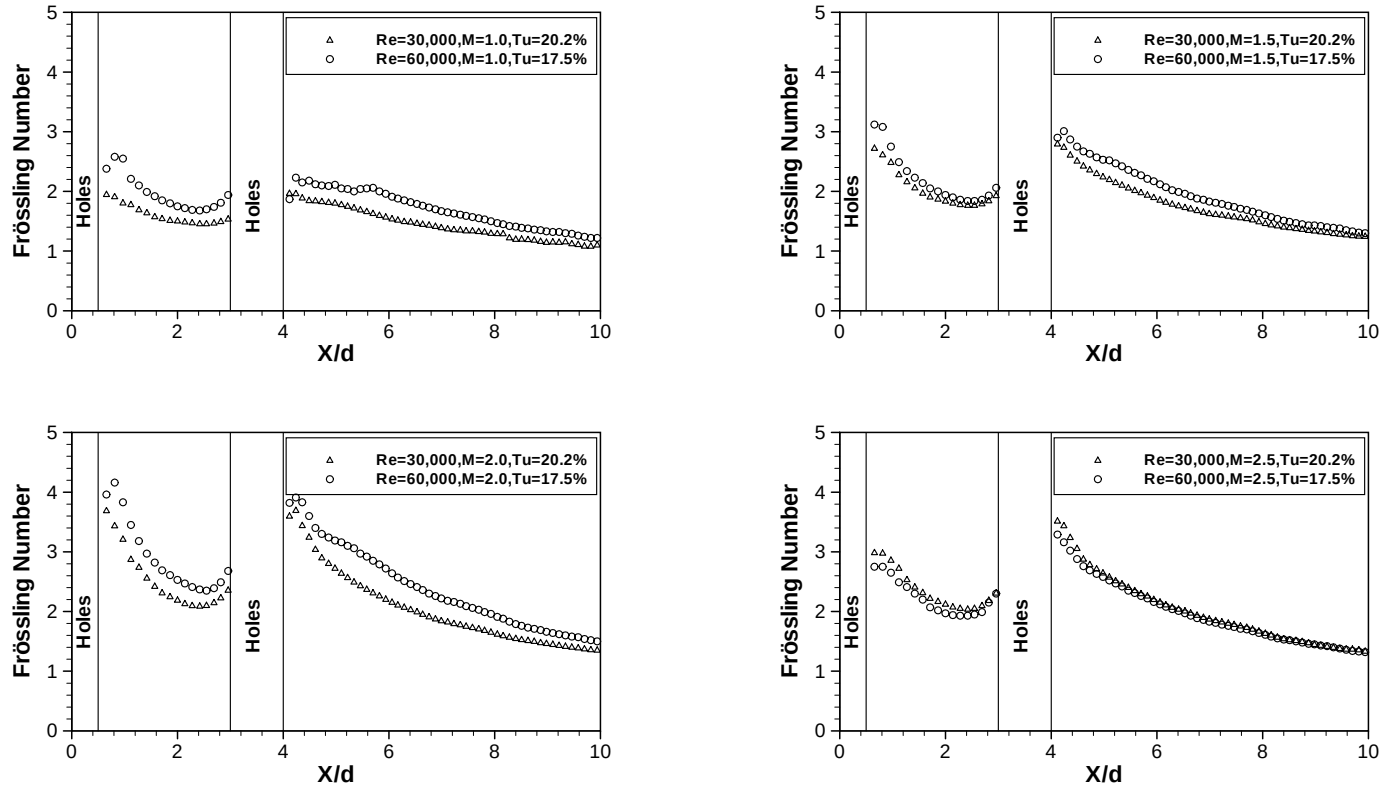

Figure 15. Effect of Reynolds Number on Spanwise Averaged Frössling Number for High Turbulence at Four Blowing Ratios (M=1.0, 1.5, 2.0, and 2.5)

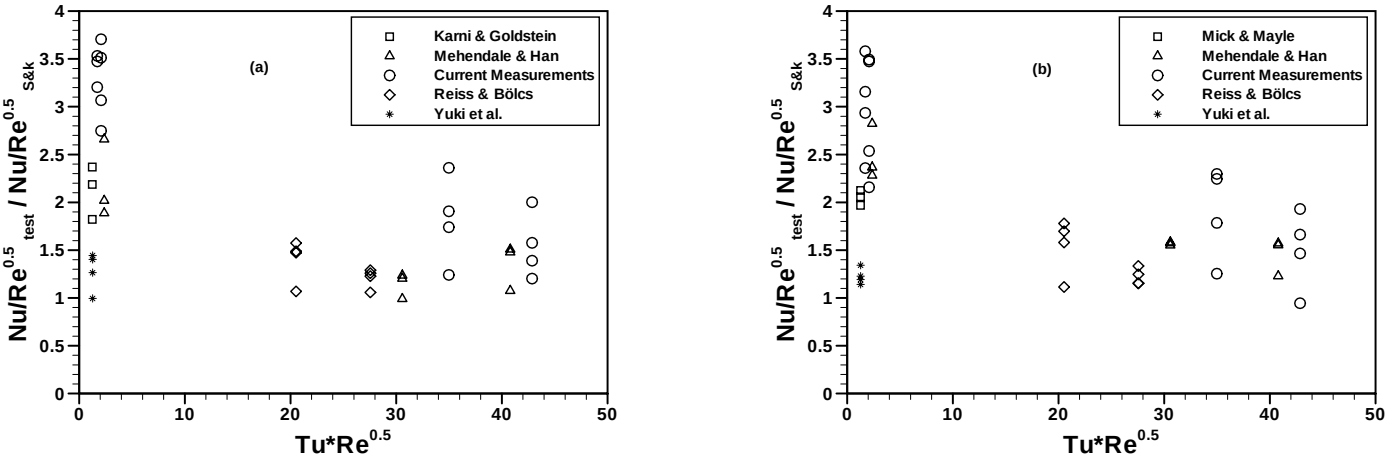

Figure 16. Comparisons of Heat Transfer Measurements with Other Results, Heat Transfer Normalized by Smith & Kuethe. (a) After First Film Row (b) After Second Film Row

SUMMARY AND CONCLUSIONS

The measured C_D's of 0.39 – 0.54 at the stagnation row of film holes for Re=30,000 show a transition from laminar to turbulent exiting velocity profiles, as the blowing ratio is increased from 1.0 to 2.5. The C_D's for Re=60,000 (0.62 to 0.69, CFD estimates $C_D \approx 0.6$) are all uniformly higher than those for Re=30,000 at stagnation row and 0.54 to 0.59 (versus 0.47 – 0.52) at 21.5º row. The calculated blowing ratios, based on the hot wire measured Umax, show a lower flow at 0º row and a higher flow at 21.5º row. Blowing ratios at the 21.5º row are higher than at the 0º row by 6% when compared to the combined nominal set point.

High turbulence intensity is shown in figure 7 to result in effectiveness attenuation of up to 60% between the rows for Re=30,000. The film effectiveness at Re = 60,000 is found to cross over to higher values after the 21.5º row in figure 8 for the high turbulence condition except for the M=1.5 case. Frössling number is only weakly effected by turbulence for Re=30,000, but turbulence still results in up to 35% reduction at Re=60,000 between the rows in figure 10 at M= 1.0. There is little turbulence effect on the Frössling number after the 21.5º row for both Reynolds numbers. Blowing ratio effects are very strong and ordered ranging to 2.8 times the M=1.0 film effectiveness between the rows for high turbulence. The Reynolds number effect is most significant for the film effectiveness at all locations for the case of M=1.0 and high turbulence. The M=2.0 case consistently shows a coupling between the stagnation row and the 21.5º row resulting in the highest film effectiveness and Frössling number.

Turbulence intensity, blowing ratio and Reynolds number are all equal players in the effects on film effectiveness and heat transfer coefficient in the stagnation region, which permits the noted crossover to higher effectiveness with high Tu. Since turbulence scale is a major effect in computations as well as experiments its role in the stagnation film cooling problem should be further defined.

ACKNOWLEDGEMENTS

This work was supported in part by Pratt & Whitney, and the Air Force Office of Scientific Research. Dr. Tom Beutner was the program manager.

REFERENCES

Burd, S.W. and Simon, T.W., 1998, "Measurements of Discharge Coefficients in Film Cooling," ASME Paper 98-GT-9.

Chernobrovkin, A. and Lakshminarayana, B., 1999, "Numerical Simulation and Aerothermal Physics of Leading Edge Film Cooling," *Proc Instn Mech Engrs* Vol 213 Part A. pp. 103-118.

Cruse, M. W., Yuki, U. M., and Bogard, D. G., 1997, "Investigation of Various Parametric Influences on Leading Edge Film Cooling," ASME Paper 97-GT-296.

Ekkad, S. V., Du, H., and Han, J. C., 1995, "Local Heat Transfer Coefficient and Film Effectiveness Distributions on a Cylindrical Leading Edge Model Using a Transient Liquid Crystal Image Method, ASME Winter Annual Meeting, San Francisco, CA.

Farina, D. J. and Moffat, R. J., 1994, "A System for Making Temperature Measurements Using Thermochromic Liquid Crystals," Thermo Sciences Division, Stanford University, Report No. HMT-48.

Giedt, W. H., 1949, "Investigation of Point Unit-Heat-Transfer Coefficient Around a Cylinder Normal to an Air Stream," *Trans. ASME*, Vol. 71, pp. 375-381.

Gritsch, M., Schulz, A., and Wittig, S., 1997, "A Method for Correlating the Discharge Coefficient of Film–Cooling Holes with Crossflows at Hole Entry and Exit," 1997 ISABE Vol. 1, pp.771-777.

Jakoby, R., Geis, T., Kim, S., and Wittig, S., 1997, "Discharge Coefficients of Rotating Orifices with Radiused Inlet Corners," 1997 ISABE Vol. 1, pp.778-786.

Karni, J. and Goldstein, R. J., 1990, "Surface Injection Effect on Mass Transfer From a Cylinder in Crossflow: A Simulation of Film Cooling in the Leading Edge Region of a Turbine Blade," *ASME Journal of Turbomachinery*, Vol. 112, pp. 418 – 427.

Kline, S. J. and McClintock, F. S., 1953, "Describing Uncertainties in Single-Sample Experiments," *Mechanical Engineering*, Jan., pp. 3-8.Lin, Y., Stephenes, M. A., and Shih, T. I-P., 1997, "Computation of Leading-Edge Film Cooling with Injection Through Rows of Compound Angle Holes," ASME Paper No. 97-GT-298.

Martin, C. A. and Thole, K. A., 1997, "A CFD Benchmark Study: Leading Edge Film-Cooling with Compound Angle Injection," ASME Paper No. 97-GT-297.

Mehendale, A. B. and Han, J. C., 1992, "Influence of High Mainstream Turbulence on Leading Edge Film Cooling Heat Transfer," *ASME Journal of Turbomachinery*, Vol. 114, pp. 707-715.

Mehendale, A. B. and Han, J. C., 1993, "Reynolds Number Effect on Leading Edge Film Effectiveness and Heat Transfer Coefficient," *International Journal of heat and Mass Transfer*, Vol. 36, No. 15, pp. 3723-3730.

Mick, W. J. and Mayle, R. E., 1988, "Stagnation Film Cooling and Heat Transfer, Including Its Effect Within the Hole Pattern," *ASME Journal of Turbomachinery*, Vol. 110, pp. 66-72.

Ou, S., Mehendale, A. B., and Han, J. C., 1992, "Influence of High Mainstream Turbulence on Leading Edge Film Cooling Heat Transfer: Effect of Film Hole Row Location", *ASME Journal of Turbomachinery*, Vol. 114, pp. 715-723.

Reiss, H. and Bölcs, A., 1999, "Experimental Study of Showerhead Cooling on a Cylinder Comparing Several Configurations Using Cylindrical and Shaped Holes," ASME Paper No. 99-GT-123.

Rivir, R. B. and Gogineni, S. P.,1996, "Characteristics of Simulated Turbine Film Cooling Flow," ASME International Congress on Fluid Dynamicss & Propulsion, Cairo, Egypt, Vol. I, pp. 95-107.

Rowbury, D. A., Oldfield, M. L. G., Lock, G. D., and Dancer, S. N., 1998, "Scaling of Film Cooling Discharge Coefficient Measurements to Engine Conditions," ASME Paper 98-GT-79.

Smith, M. C. and Kuethe, A. M., 1966, "Effects of Turbulence on Laminar Skin Friction and Heat Transfer," *The Physics of Fluids*, Vol. 9, No. 12, pp. 2337-2344.

Thole, K., 2000, private communication, Virginia Polytech Institute & State University.

Thakur, S., Wright, J., and Shyy, W., 1997, "Computation of a Leading Edge Film Cooling Over an Experimental Geometry," ASME Paper No. 97-GT-381.

VanFossen, G. J. and Ching, C. Y., 1994, "Measurements of the Influence of Integral Length Scale on Stagnation Region Heat Transfer," *NASA Technical Memorandum 106503.*

Vedula, R. J. and Metzger, D. E., 1991, "A Method for the Simultaneous Determination of Local Effectiveness and Heat Transfer Distributions in Three-Temperature Convection Situations," ASME Paper No. 91-GT-345.

Yuki, U. M., Bogard, D. G., and Cutbirth, J. M., 1998, "Effect of Coolant Injection on Heat Transfer for a Simulated Turbine Airfoil Leading Edge," ASME Paper No. 98-GT-431.